Composites: Part A 85 (2016) 181–191

Contents lists available at ScienceDirect

Composites: Part A

journal homepage: www.elsevier.com/locate/compositesa

Fused deposition modelling with ABS–graphene nanocomposites

Sithiprumnea Dul, Luca Fambri, Alessandro Pegoretti *

Department of Industrial Engineering and INSTM Research Unit, University of Trento, Via Sommarive 9, 38123 Trento, Italy

ARTICLE INFO

Article history:
Received 9 December 2015
Received in revised form 10 February 2016
Accepted 16 March 2016
Available online 21 March 2016

Keywords:
A. Graphene
B. Mechanical properties
C. Creep
Fused deposition modelling

ABSTRACT

For the first time, graphene nanoplatelets (xGnP) were incorporated at 4 wt% in acrylonitrile–butadiene–styrene (ABS) filaments obtained by a solvent-free process consisting of melt compounding and extrusion. Nanocomposite filaments were then used to feed a fused deposition modelling (FDM) machine to obtain specimens with various build orientations. The elastic modulus and dynamic storage moduli of 3D printed parts along three different build orientations were increased by the presence of xGnP in the ABS matrix. At the same time, a decrease in both stress and strain at break was observed when xGnP is added to ABS. Moreover, a higher thermal stability was induced on 3D printed parts by xGnP, as indicated by a reduction in both coefficient of linear thermal expansion and creep compliance. A comparison between 3D printed and compression moulded parts highlighted the importance of the orientation effects induced by the fused deposition modelling process.

1. Introduction

Additive manufacturing (AM) is a technology of building objects layer-by-layer based on computer aided design (CAD) [1]. This technology attracts strong interest from both industry and academic for the challenging possibility to build objects with complex shapes and minimal use of harmful chemicals at a reasonable speed [2–5]. Among AM methods, fused deposition modelling (FDM) is one of the most common techniques. In this process, a filament of a thermoplastic polymer is extruded at above its glass transition or melting temperature though a nozzle and deposited layer-by-layer on a platform to build the tridimensional (3D) object. In fact the term 3D printing is frequently used to refer to this technology. The most frequently used thermoplastic polymers are acrylonitrile–butadiene–styrene (ABS) and polylactic acid (PLA), but also polycaprolactone (PCL) and polycarbonate (PC) have been considered [6–9]. Single, double, or even triple-head 3D printing machines have been used with different polymers in order to modulate the properties, as described by Leigh et al. [10] with ABS, PLA and PCL. One of the main limitations of this AM technique is related to the limited mechanical properties of the 3D printed parts [11–13].

Development of composite materials could be a way to improve the mechanical properties of components produced by FDM. In recent years, polymer nanocomposites (PNCs) have attracted attention due to the possibility of improving the properties of host matrices with a small amount of filler. Adding nanomaterials such as carbon nanotubes, nanowires, and nanoparticles to matrices such as polymers, metals, and ceramics via AM has the potential to improve the performances of the resulting components [3,14].

A quite limited amount of information are available in the open scientific literature on the development of ABS-based micro or nanocomposites for FDM application. In particular, reinforcing materials have been considered in form of spherical particles (such as titanium dioxide [13] or fumed silica [15]), microfibers (such as jute fibres [13], short glass fibres [16] and carbon fibres [11,12]) nanofibers (such as vapour-grown carbon fibres [17]), carbon nanotubes [18–21] and nanoclays [22].

Recently, graphene nanoplatelets (xGnP) are under investigation as potential reinforcing fillers for polymer based nanocomposites. Graphene nanoplatelets are ultrathin particles consisting of short stacks of graphene sheets. This kind of nanofiller has been used as multifunctional reinforcement, because it possesses 2D graphene stacked structure resulting in superior mechanical, electrical and thermal properties. Therefore, for thermoplastic nanocomposite filled with xGnP dramatic enhancements of mechanical properties and thermal stabilities were reported [23–29].

To the best of our knowledge, only one paper has been recently published in the open scientific literature regarding the addition of graphene platelets as nanofillers in ABS for FDM applications [30]. Fully exfoliated GO sheets and ABS were mixed in solution in a solvent (N-methyl-pyrrolidone) up to a concentration of 5.6 wt%. The GO sheets were chemically reduced and the resulting nanocomposites extruded in filaments used to feed a FDM machine. Even

* Corresponding author.
E-mail address: alessandro.pegoretti@unitn.it (A. Pegoretti).

http://dx.doi.org/10.1016/j.compositesa.2016.03.013
1359-835X/

of the mechanical properties were not investigated, for the 3D printed samples containing graphene a very slight decrease of the coefficient of linear thermal expansion (by about 4%) was reported along with a reduction of the loss factor.

In the present study, graphene–ABS filaments suitable for a FDM process were produced through a solvent-free procedure based on melt compounding and extrusion. In order to select an optimal xGnP content for melt compounding and extrusion, a preliminary study was conducted in terms of tensile mechanical properties and melt flow index (MFI) test. The properties of neat ABS and ABS-xGnP nanocomposites were monitored on samples obtained by compression moulding, extruded filament and FDM-printed parts. Moreover, the effect of xGnP on ABS parts was investigated along three different building orientations (i.e. horizontal, vertical and perpendicular) among those possible for the FDM process.

2. Experimental

2.1. Materials

Acrylonitrile–butadiene–styrene (ABS) polymer (tradename Sinkral® PD L 322) was provided by Versalis S.p.A. (Mantova, Italy) in form of white pellets. According to the producer's technical data sheet the material is characterized by a density of 1.04 g/cm^3 and a melt flow index of 23 g/10 min (220 °C/10 kg). The two ABS phases, i.e. glassy styrene–acrylonitrile (SAN) phase and rubbery butadiene (B) phase were analysed by differential scanning calorimetry and by dynamical mechanical analysis.

Graphene nanoplatelets (xGnPs) were purchased from XG Sciences (East Lansing, MI). For the selected type of nanoplatelets (type M5), the manufacturer reports average lateral dimension of 5 μm, thickness in the range 6–8 nm, surface area of 120–150 m^2/g and bulk density of 2.2 g/cm^3.

2.2. Materials processing and sample preparations

2.2.1. Compounding

Various amounts (2, 4 and 8 wt%) of xGnPs were melt compounded with ABS by a Thermo-Haake Polylab Rheomix counter-rotating internal mixer at 190 °C, rotor speed 90 rpm for 15 min. ABS was melted in the first 4 min, and after the addition of graphene (at minute 5) a direct increase of torque was observed, followed by a slight decrease of torque up to minute 6 due to a partial degradation of ABS matrix. Then in the last 9 min of compounding, a constancy in the torque value suggested the absence of further degradation of the matrix and the leveling of filler's dispersion. Neat ABS was also processed under the same conditions. Three batches of about 50 g were processed for each composition and the resulting material was granulated in a Piovan grinder Model RN 166.

2.2.2. Compression moulding (CM)

Compounded materials were hot pressed in a Carver Laboratory press at a temperature of 190 °C under a pressure of 3.9 MPa applied for 10 min and a cooling rate of 20 °C/min to obtain square plaques with dimensions 160 × 160 × 1.2 mm. Compression moulded samples will be identified with the code CM.

2.2.3. Filament extrusion

Compounded materials were also used to feed a Thermo Haake PTW16 intermeshing co-rotating twin screw extruder (screw diameter = 16 mm; L/D ratio = 25; rod die diameter 3 mm). The processing temperature gradually increased from 180 °C (zone 1), to 190 °C (zone 2), to 195 °C (zones 3 and 4) to 200 °C (zone 5 – rod die). The screw rotation speed and collection rate were regulated in order to obtain a final diameter of the extruded filament of 1.75 ± 0.10 mm with an output of 195–200 g/h. Screw speed at 9 and 10 rpm, and pressure of about 6.7 and 7.8 bar were selected for neat ABS and graphene nanocomposite extrusion, respectively. A constant collection rate of 1.3 m/min was imposed by using a take-up unit Thermo Electron Type 002-5341. The code E will be used to identify extruded filament samples.

2.2.4. FDM printed samples preparation

3D printed specimens were manufactured by a Sharebot Next Generation desktop 3D printer (Sharebot NG, Italy) feed with the filaments extruded as described in the previous paragraph.

As schematically represented in Fig. 1, dumbbell and parallelepiped specimens were built-up along three different orientations, i.e. horizontal, vertical and perpendicular, and coded as H, V and P, respectively. X is the direction of filament deposition and Z is the direction of the overlapping layers.

Infill type of concentric and maximum fill percentage were used in Slic3r software along with the following printing parameters: concentric type of infill; object infill 100%; no raft; nozzle diameter 0.35 mm; layer height 0.20 mm; nozzle temperature 230 °C; bed temperature 60 °C. The deposition rate has been fixed at 40 mm/s for H and V samples, whereas P specimens were produced at lower deposition rate (4 mm/s) in order to allow the solidification of deposited beads and provide a support for the growing part. For V specimens it was necessary to generate a support material deposited at 50 mm/s. The size and the processing parameters of FDM specimens are summarized in Table 1.

2.3. Testing techniques

2.3.1. Scanning electron microscopy

The fracture surfaces were observed through a Carl Zeiss AG Supra 40 field emission scanning electron microscope (FESEM), operating at an acceleration voltage of 5 kV. Specimens were immersed in liquid nitrogen for about 60 min and broken in a brittle manner.

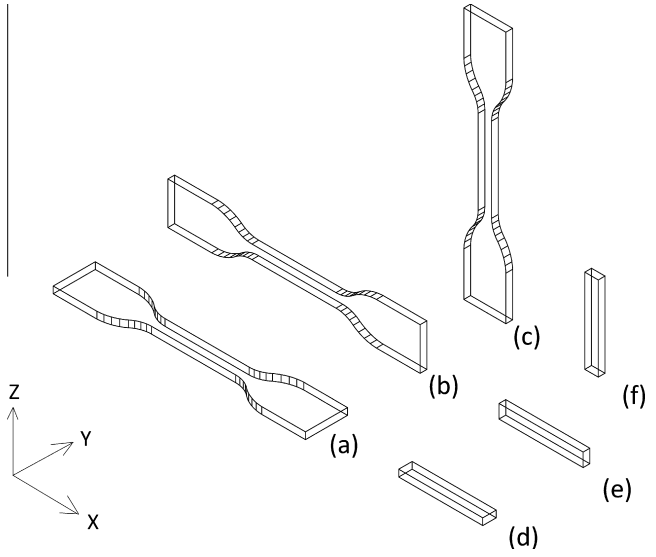

Fig. 1. Schematic of 3D-printed dumbbell and parallelepiped specimens at different orientations: (a) and (d) horizontal (H); (b) and (e) vertical (V); (c) and (f) perpendicular (P).

Table 1
Dimensions and processing parameters of FDM specimens.

Sample	X (mm)	Y (mm)	Z (mm)	F [b] filaments in a layer	D deposition time of a single layer (s)	D/F deposition time of a single filament (s)	Number of layers	Total time [c] (min)	Analysis
Dumbbell									
H	75	4–12.5[a]	2	11	43	4	10	8	Tensile test
V	75	2	4–12.5[a]	5	21	4	20–63	14	Tensile test
P	4–12.5[a]	2	75	5	11	2	375	89	Tensile test
Parallelepiped									
H	25	4	1	11	10	1	5	1.2	Creep
	25	4	2	11	10	1	10	2	DMA
V	25	1	4	3	4	1	20	1.6	Creep
	25	2	4	5	5	1	20	2.1	DMA
P	1	4	25	3	6	2	125	15	Creep
	2	4	25	5	9	2	125	21	DMA

[a] min and max values of specimen's width are reported.
[b] Number of contiguous filaments in a single layer in the gage length.
[c] For production of one FDM specimen taking into account non-print moves of nozzle.

2.3.2. Differential scanning calorimetry

Differential scanning calorimetry (DSC) tests were performed by a Mettler DSC 30 calorimeter under nitrogen flow of 100 ml/min on samples with a mass of about 10 mg. The samples were first heated from 30 °C to 260 °C at a rate of 10 °C /min followed by an isothermal stay at 260 °C for 5 min. The samples were then cooled down from 260 °C to 30 °C at a rate of −10 °C /min and re-heated at the same rate from 30 °C to 260 °C. Glass transition temperature (T_g) of SAN phase was measured as inflection point of the thermogram.

2.3.3. Melt flow index

The melt flow index (MFI) measurements were carried out according to ASTM D 1238 standard (procedure A), through a Kayeness Co. model 4003DE capillary rheometer, at a temperature of 220 °C with an applied load of 10 kg.

2.3.4. Quasi-static tensile test

Uniaxial tensile tests were carried out at room temperature by an Instron® 5969 electromechanical testing machine equipped with a 50 kN load cell.

Ultimate strength (σ_b) and strain at break (ε_b) were evaluated at a crosshead speed of 10 mm/min as average value of at least three replicates. Specimens consisted of (i) compression moulded (CM) materials ISO 527 type 1BA dumbbell (gauge length 30 mm; thickness 1.2 mm); (ii) extruded filaments (E) (gauge length 100 mm diameter 1.75 mm); (iii) 3D printed materials (H, V and P), ISO 527 type 5A dumbbell (gauge length 25 mm; thickness 2 mm).

Elastic modulus of CM and 3D-printed H, V and P specimens was determined at a cross-head speed of 1 mm/min by an electrical extensometer Instron® model 2620-601 with a gage length of 12.5 mm; whereas the modulus of E specimens was measured at a cross-head speed of 10 mm/min without extensometer with a gage length of 100 mm taking the system compliance into account. According to ISO 527 standard, the elastic modulus was determined as a secant value between strain levels of 0.05% and 0.25%.

2.3.5. Dynamic mechanical thermal analysis

Dynamic mechanical thermal analysis (DMA) tests were performed under tensile mode by a TA Instruments DMA Q800 device. For CM and 3D-printed materials, rectangular specimens were tested with a length of 25 mm, and different cross section (width 5 mm and a thickness 1.2 mm for CM and width 4 mm and a thickness 2 mm for 3D-printed materials). Extruded filaments 25 mm in length and a diameter of 1.75 mm were tested. The gauge length of all samples was fixed at 11.8 mm. Tests were performed from −100 °C to 150 °C at a heating rate of 3 °C/min applying a dynamic maximum strain of 0.05% at a frequency of 1 Hz. Storage modulus (E'), loss modulus (E'') and loss tangent ($\tan\delta$) as a function of the temperature were reported. From the thermal strain curve, a coefficient of linear thermal expansion (CLTE) below T_g and a coefficient of linear thermal deformation (CLTD) above T_g were determined according to Eq. (1):

$$\text{CLTE (or CLTD)} = \frac{\Delta L/L_0}{\Delta T} \quad (1)$$

where L_0 and ΔL are the initial specimen gauge length and the length variation, and ΔT is the selected temperature interval (i.e. −50/−20 °C; 20/50 °C; 70/90 °C, 108 °C/113 °C for CLTE and 120/150 °C for CLTD).

2.3.6. Creep test

Creep test were preformed through a TA Instruments DMA Q800 under a constant stress of 3.9 MPa (i.e. about 10% of yield stress of neat ABS) at 30 °C up to 3600 s. Rectangular samples with length of 25 mm, width of 5 mm and thickness of 0.9 mm were machined from compression moulded plaques. Cylindrical extruded specimen with diameter 1.75 mm with length of 25 mm were used. Rectangular specimens with length of 25 mm, width of 4 mm and thickness of 1 mm were also prepared by 3D printing. The adopted gauge length of all samples was 11.8 mm.

3. Results and discussions

3.1. Optimization of xGnP content

A preliminary study was performed to select an optimal concentration of graphene nanoplatelets in the ABS matrix for the intended application. Graphene nanoplatelets were melt-compounded with ABS and plaques were compression moulded as described in the Experimental section. Fig. 2 summarizes the tensile mechanical properties and melt flow index values determined on the CM materials as a function of the xGnP content. The elastic modulus of nanocomposite materials increases with the amount of xGnP. On the other hand, the tensile strength of materials slightly decreases when the xGnP concentration increases. At the same time, a remarkable reduction of the deformation at break can be observed when xGnP nanoparticles are added. This experimental evidence could be attributed to a poor adhesion level between the xGnP nanoplatelets and the ABS

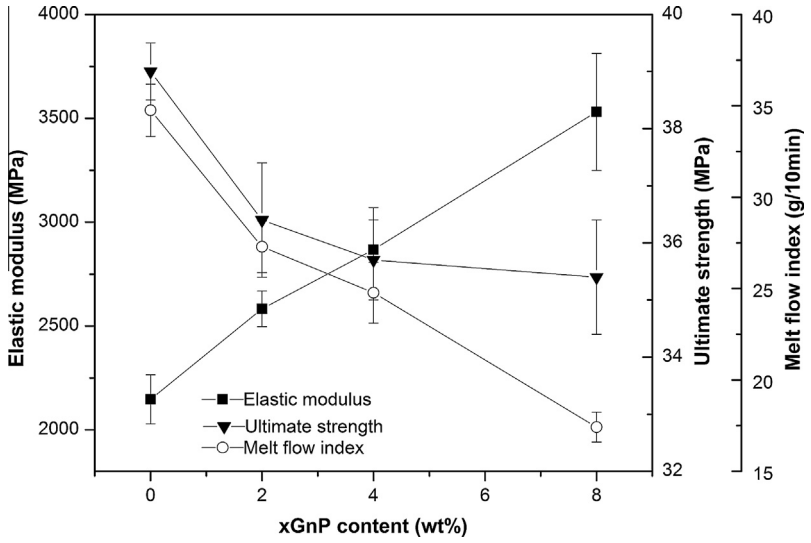

Fig. 2. Tensile modulus, tensile strength and melt flow index values for compression moulded neat ABS and ABS-xGnP nanocomposites.

matrix. It is worthwhile to observe that the MFI values strongly decrease with the xGnP content due to the increasing viscosity in nanocomposites induced by the formation of a nanofiller network, as documented by the torque increase after addition of graphene to ABS in melt-compounding process. Considering the necessity of extruding filaments for the 3D printing process, the viscosity cannot be too high and therefore a graphene nanoplatelets content of 4 wt% has been considered to be an optimal value. Therefore, all the subsequent investigations have been limited to nanocomposites containing 4 wt% of xGnP and the corresponding samples were identified with a code starting with 4.

3.2. Filament extrusion

Filaments of ABS and ABS with 4 wt% of graphene nanoplatelets were extruded with an apparent draw ratio (ADR) of 2.95 calculated, according to Eq. (2), as the ratio between the cross sectional area of the extrusion die (S_D) and the cross sectional area of the filament (S_F).

$$ADR = S_D/S_F \quad (2)$$

The apparent draw ratio includes the effect of die-swelling (DS), i.e. the ratio between the cross sectional area of extrudate (S_E) and the cross sectional area of the die.

$$DS = S_E/S_D \quad (3)$$

For nanocomposite filaments a lower DS value (1.19) was experimentally determined with respect to neat ABS that presented a value of 1.34. This difference could be attributed to the effect of graphene nanoplatelets on the rheological behaviour of the investigate material. Combining Eqs. (2) and (3), an effective draw ratio (DR) can be calculated as:

$$DR = ADR \cdot DS = S_E/S_F \quad (4)$$

DR values of 3.9 and 3.5 were evaluated for ABS (E) and nanocomposite (4-E) filaments, respectively.

About 40 m of ABS (E) and nanocomposite (4-E) filaments were produced with linear density of 2490 ± 143 tex and 2516 ± 145 tex, respectively [31]. Corresponding bulk density of 1.036 ± 0.008 g/cm^3 and 1.049 ± 0.016 g/cm^3 were also estimated from direct measurement of filament weight and volume.

Extruded nanocomposite filaments were less flexible and more brittle than unfilled ABS filaments, and for this reason were wounded onto spools with diameter of 20 cm, instead of spools with 10 cm diameter suitable for standard ABS, in order to avoid fracture of filament during the printing process.

3.3. Microstructure and differential scanning calorimetry

Fig. 3a–c shows low magnification FESEM pictures of the fracture surface of neat ABS of H, V and P dumbbell specimens, respectively. Identification of the FDM process parameters significantly affecting the quality of FDM processed parts is of primary importance [32]. In Fig. 3a and b the cross-sections of single filaments in samples H and V can be observed; the trapezoidal shape (final thickness of 0.20 mm and width of about 0.41 mm), indicates not only a shape variation from the initial circular section (nozzle diameter of 0.35 mm), but also a slight reduction of the filament cross-section due to the polymer orientation during FDM process. In particular, a draw ratio of 1.2 could be estimated as the ratio between the original section of the filament at the nozzle and the average section measured from Fig. 3a and b. This drawing is expected to improve the mechanical properties along the correspondent direction (X), as direct consequence of the orientation of polymer chains [33]. Of course, the above considerations do most probably underestimate the drawing of the filament during the FDM process since any filament expansion when it leaves the nozzle is neglected. Moreover, the coalescence of material showed in the upper level determines an almost flat plane for the next layer deposition; whereas the lack of continuity is evident in triangular cavities at the base of deposition plane. Sample V has been built-up by layering five contiguous filaments that have been deposited as follows: first the external frame (filaments 1 and 5), then the infill process with an inner concentric frame (filaments 2 and 4) and the last third filament in the middle. Fig. 3b shows some defects between the second and the third filament (see highlighted zone in Fig. 3b), evidencing a non-regular co-contiguity in the middle part of the layer; however these small local imperfections do not compromise the mechanical performances of the sample. On the other hand, the fracture surface of sample P (Fig. 3c) indicates a brittle fracture of an almost homogeneous material, and no traces of the precursor filament are evident. This suggests that deposited filaments completely merge together in kind of single coalesced layers, due to the shorter time of deposition of contiguous filaments in the plane X–Y. Moreover, the total deposition time of five filaments of a layer in sample P is 11 s (Table 1), much faster than

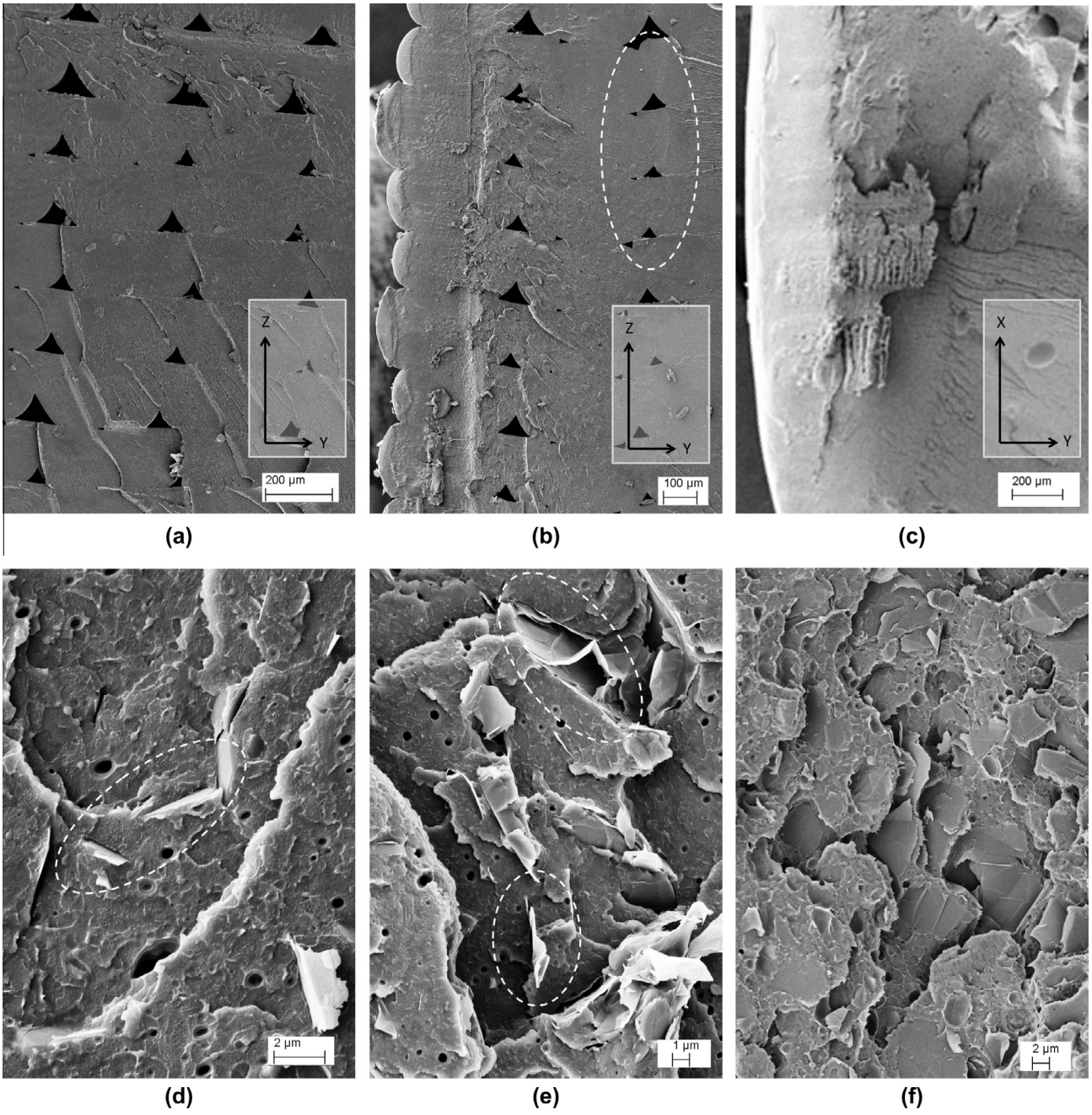

Fig. 3. SEM micrographs of 3D-printed dumbbell specimens printed from neat ABS, H (a), V (b) and P (c); and from graphene nanocomposites, 4-H (d), 4-V (e) and 4-P (f).

that of samples H and V. Taking into account the number of filaments, about 4 s is the average time between the contact deposition in dumbbell specimens H and V, whereas for sample P the average time is about 2 s. This processing time is even lower in parallelepiped specimens (about 1–2 s). The shorter the time, the better the interaction and inter-joining between contiguous filaments, because the filament temperature is higher and closer to the polymer T_g, determining a higher quality of filament bonding [34].

FESEM pictures at higher magnification of the cross-section of the 3D-printed dumbbell specimens of ABS/graphene nanocomposite are reported for horizontal, vertical and perpendicular orientation, in Fig. 3d, e and f, respectively. According to Fig. 3d and e, the graphene nanoplatelets for H and V parts appear to be mostly perpendicular to the fracture plane and therefore most likely oriented along the loading direction of dumbbell specimens. On other hand, Fig. 3f clearly proves that in P specimens, graphene nanoplatelets appear to be distributed parallel to the cross-section. It can be therefore inferred that, during FDM process, the graphene nanoplatelets are forced to align along the layer plane. A relatively good dispersion of graphene nanoplatelets in ABS matrix can be observed for all building directions.

Fig. 4 shows the typical DSC thermograms of compression moulded specimens, extruded filaments and 3D printed H specimens of neat ABS and nanocomposites. Two transitions are clearly visible both in the first (Fig. 4a) and in the second heating scan (Fig. 4c), i.e. the glass transition temperature of styrene–acrylonitrile copolymer phase (SAN) at about 105 °C (in conformity to literature indications [30,35]), followed by an endothermic peak at

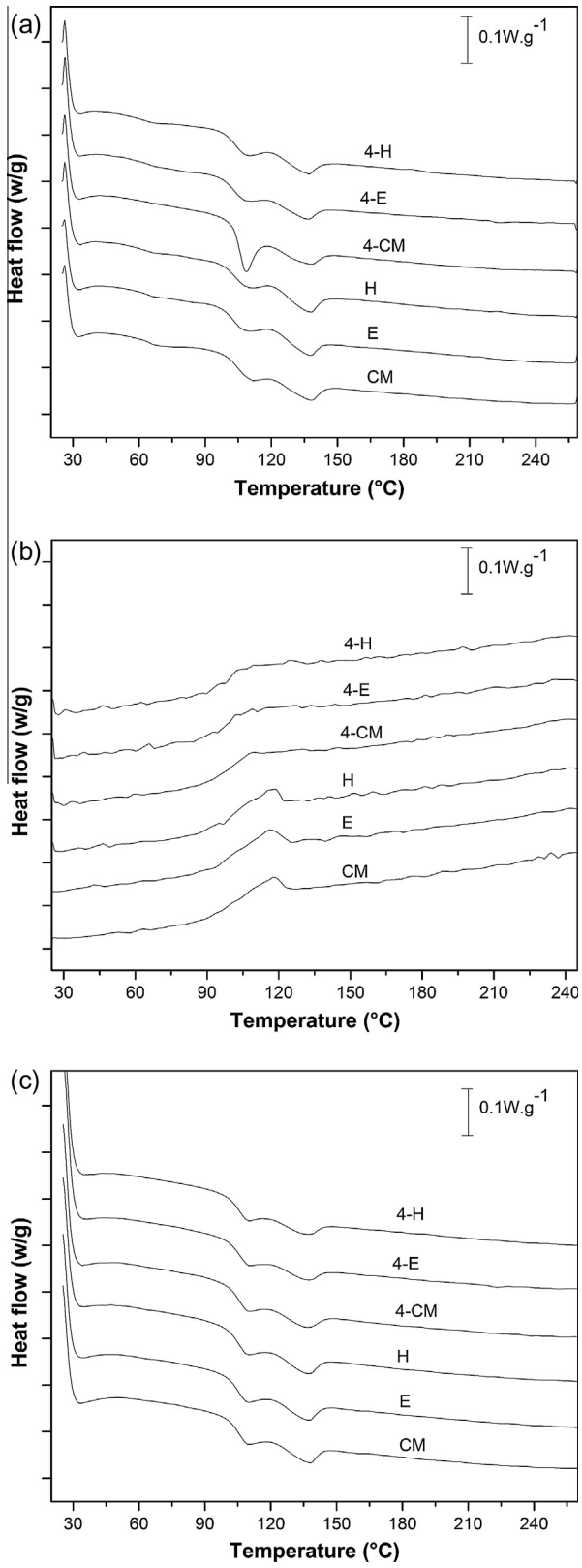

Fig. 4. DSC thermograms of neat ABS and nanocomposite. First heating scan (a), cooling scan (b), and second heating scan (c) of CM (compression moulded), E (extruded) and FDM specimens.

about 140 °C. Differently from the interpretation provided by Rytlewski et al. [36], in our opinion this endothermal peak cannot be attributed to the melting of acrylonitrile AN crystallites, but it is most probably related to a mould lubricant that is generally added for better processing of commercial high viscosity ABS, as described by Reed et al. [37].

In Table 2, the T_g of SAN phase and data of melting (T_m, ΔH_m) and crystallization (T_c, ΔH_c) of mould lubricant are summarized. The transition temperatures T_g and T_m for pure ABS were fairly constant at about 105 °C and 137 °C, respectively, independently from the processing technique. Addition of xGnP did not significantly affect the glass transition temperature measured by DSC. On the other hand, no crystallization peak was found in the cooling step of nanocomposites (thermograms shown in Fig. 4b; see data in Table 2). However, the melting peak in the second heating scan (Fig. 4c) suggests that graphene could favour the progressive crystallization of the lubricant and to play a nucleating effect on it.

3.4. Quasi-static tensile tests

The effect of xGnP nanoplatelets on the elastic modulus (E), tensile strength (σ_b) and strain at break (ε_b) of neat ABS and ABS nanocomposite compression moulded, extruded and 3D-printed parts with different orientations are summarized in Table 3. In general, it can be noted how the presence of graphene nanoplatelets promotes a remarkable increase of the elastic modulus of the ABS matrix, but slightly decreases its ultimate tensile strength. Concurrently, a noticeable drop of the strain at break values can be observed when xGnP nanoparticles are added. The reduction of ultimate properties could be attributed to a poor adhesion level between the nanofiller and ABS matrix as documented by the FESEM observations of Fig. 3.

As it clearly emerges from Table 3, for neat ABS the elastic modulus of compression moulded samples is higher than that of 3D-printed samples along horizontal direction (sample H). This behaviour could be explained by the fact that a compaction pressure is applied only in the compression moulding process, while both extrusion and FDM processes are characterized by low or no compaction pressure. On the other hand, the almost similar elastic modulus of CM and E parts could be the result of two opposite factors: from one side the underestimation of true strain in tensile test on E samples due to the impossibility of using a contact extensometer, and from the other side the positive effect of orientation during extrusion. Moreover, for 3D-printed specimens the presence of voids (about 6 vol% as observed from Fig. 3a) in the microstructure leads to a lower effective cross-section. The strength values of neat ABS compression moulded samples is of about 39 MPa and it remains almost constant on both extruded filaments and FDM samples along horizontal direction (sample H). Tekinalp et al. also reported similar tensile strength values for neat ABS processed by CM or FDM [12].

Upon addition of 4 wt% of xGnP the elastic modulus improves by about 30% compared to unfilled ABS for all the investigated processing conditions, i.e. CM, extruded and horizontally oriented 3D printed samples. As expected, the build orientation remarkably

Table 2
Glass transition temperatures of styrene–acrylonitrile phase (T_g), melting temperature (T_m) and enthalpy of fusion of lubricant (ΔH_m), crystallization temperature (T_c) and crystallization enthalpy (ΔH_c) for ABS and relative nanocomposite from DSC.

Sample	First heating			Cooling		Second heating		
	T_g (°C)	T_m (°C)	ΔH_m (J/g)	T_c (°C)	ΔH_c (J/g)	T_g (°C)	T_m (°C)	ΔH_m (J/g)
CM	104.8	137.8	3.0	117.8	2.3	105.6	137.6	2.5
E	102.2	137.5	3.1	116.2	2.4	105.5	137.3	2.6
H	103.8	137.7	3.4	115.3	2.6	105.7	137.0	2.7
4-CM	105.6	137.4	2.5	–	–	105.8	136.5	2.3
4-E	103.2	136.8	2.6	–	–	106.0	137.2	2.0
4-H	103.7	136.8	2.7	–	–	105.5	136.9	2.0

Table 3
Quasi-static tensile properties of ABS and its nanocomposite as measured on compression moulded (CM), extruded (E) and 3D-printed specimens with different orientations (H, V, P).

Sample	E (MPa)	σ_b (MPa)	ε_b (%)
CM	2147 ± 118	39.0 ± 0.5	28.4 ± 5.2
4-CM	2868 ± 202	35.7 ± 0.7	5.1 ± 1.5
E	2080 ± 68	39.3 ± 1.2	32.5 ± 9.8
4-E	2563 ± 93	37.3 ± 0.7	3.2 ± 1.4
H	1866 ± 118	38.8 ± 0.8	4.2 ± 0.2
4-H	2463 ± 76	35.9 ± 1.0	3.0 ± 0.1
V	1687 ± 104	35.7 ± 2.4	4.5 ± 0.2
4-V	2151 ± 78	30.5 ± 0.9	3.4 ± 0.5
P	1560 ± 85	23.8 ± 1.3	3.3 ± 1.0
4-P	1686 ± 129	13.4 ± 1.3	1.8 ± 0.4

affects the tensile mechanical properties of 3D printed samples. In fact, as reported in Table 3, the horizontally built sample exhibits the highest elastic modulus and ultimate strength, followed by vertical and then by perpendicular parts, respectively. Also of H and V samples results to be higher than that of P sample. The behaviour observed for H and V samples is certainly related to the direction of the deposited filaments preferentially aligned along the tensile applied load, while the deposited beads in P specimens are mostly oriented transversally to the tensile load. According to the existing literature information on the effects of build orientation on the elastic modulus and tensile strength of ABS 3D printed parts similar trends were reported [2,13,38]. Valentan et al. [39] reported a significant effect of nozzle temperature on tensile elastic modulus and strength. Complementary information on mechanical properties of ABS FDM samples as a function of building directions were also reported by Jami et al. [40].

As summarized in Table 3, the addition of xGnP induces an improvement of the elastic modulus by 32%, 28% and 8% for H, V and P samples, respectively. Kim et al. [26] observed that the tensile moduli of xGnP-PA6 composite fibres showed significant improvements over bulk materials attributed to the drawing induced alignment of PA6 molecular chains as well as the alignment of xGnPs. Our results also suggest that the filler plays the best reinforcement efficiency when the deposited beads lie parallel to tensile load, because the filament orientation induce a certain alignment of graphene platelets along the extrusion direction (see the dotted zones in Fig. 3d and e).

Concerning the ultimate properties, FDM sample built in perpendicular direction exhibit strength values much lower than those along horizontal and vertical directions. Fracture occurs in between two layers, and hence the tensile strength of about 24 and 13 MPa could be considered as an indication of the tensile bonding strength of neat ABS and graphene composites in FDM deposited layers, respectively. At the same time, deformation at break decreases from 3.3% to 1.8% after addition of graphene, suggesting that the interlayer bonding could be significantly reduced by the higher viscosity in molten state. Moreover, other possible reasons for the observed reduction in interlayer bonding could be related to local stress concentration induced by graphene nanoplatelets and to the intrinsically brittle nature of graphene nanoplatelets.

3.5. Dynamic mechanical response and coefficient of thermal expansion

Dynamic mechanical thermograms of ABS and its nanocomposite after compression moulding, extrusion and 3D-printing with different orientations are shown in Figs. 5 and 6, respectively. In Table 4, selected values of storage modulus (E'), loss modulus (E'') and glass transition temperature from loss tangent ($\tan\delta$) are

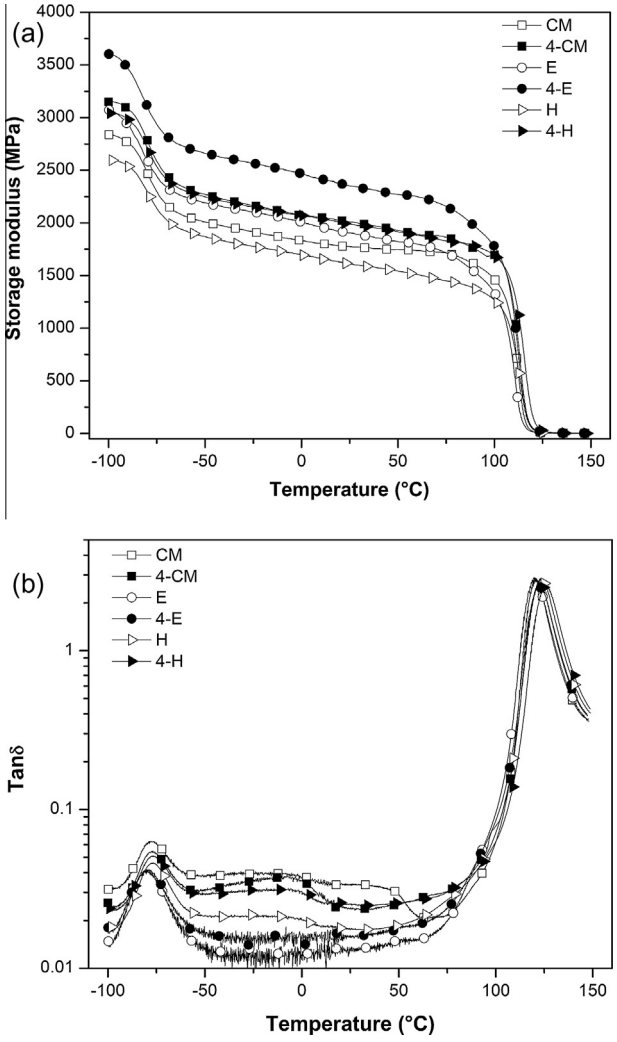

Fig. 5. Dynamic mechanical thermograms (a) storage modulus (E') and (b) loss tangent ($\tan\delta$), of neat ABS and nanocomposite samples as measured on compression moulded (CM), extruded (E) and 3D-printed specimens along horizontal orientation (H).

summarized. Due to the orientation of polymer chains during extrusion, in the entire temperature range the storage modulus of extrudate (E) is higher than that of compression moulded samples and FDM printed parts (Fig. 5a). In FDM samples the positive effect of filament orientation are counterbalanced by the negative effect of some cavities, as shown in cross section micrographs (Fig. 3a and b).

Due to the xGnP addition in the ABS matrix, the storage modulus of CM, extrudate and FDM parts increases of about 30–50% with respect to the neat ABS below the T_g. The effect of xGnP nanofiller is manifestly more evident above T_g. In fact, as shown in Table 4, the storage modulus of composite materials at 125 °C is more than twice that of neat ABS for all investigated samples, thus revealing a positive stiffening effect of graphene nanoplatelets in the molten state.

Two damping peaks can be clearly observed in Fig. 5b and b as expected in ABS copolymers. In particular, the first peak at about −76 °C is related to the glass transition temperature (T_{g1}) of the butadiene rich phase [41], while the second transition (T_{g2}) at about 120 °C is associated to the styrene–acrylonitrile (SAN) rich phase.

For all processing routes, the presence of the xGnP causes an increase of T_{g1} values by about 1 °C and T_{g2} values by about 2 °C

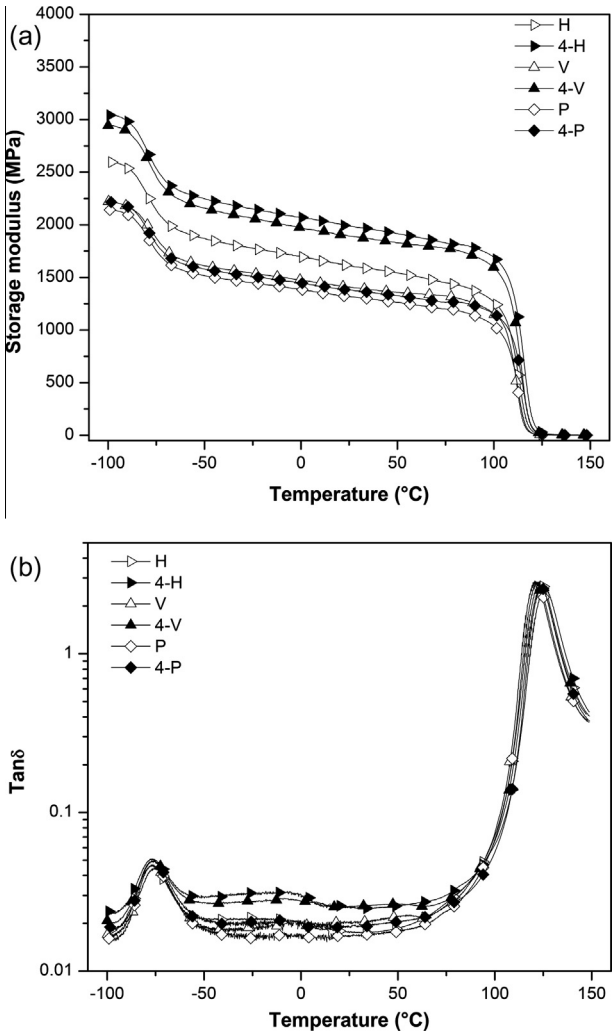

Fig. 6. Dynamic mechanical thermograms a) storage modulus (E') and b) loss factor (tanδ) of neat ABS and nanocomposite as measured on 3D-printed specimens along different orientations (H, V, P).

due to the restriction of motion of macromolecules. This observation agrees with what reported by Wei et al. [30] on a shift from 105 °C to about 106 °C for SAN phase transition after addition of 3.5% of graphene in fused deposition modelled ABS.

It is worth noting that the position of the glass to rubbery transition damping peak in ABS has been observed in the range 100–124 °C [42–44] and it does depend on various factors, such as copolymer composition, molecular weight and additives.

DMA parameters of FDM samples at various build orientations are also compared in Table 4. Horizontally built specimens show the highest storage modulus followed by vertical and perpendicular specimens, respectively. The trend is the same previously observed for the tensile Young's modulus, thus confirming that, as recently reported by Arivazhagan and Masood [45], dynamic mechanical properties strongly depend on the deposition orientation in FDM. Addition of xGnP causes an increase of the storage modulus in comparison to neat ABS for all build orientation parts: at room temperature the storage modulus increases by 23%, 34% and 5% for H, V and P orientation respectively. Therefore, it is confirmed that graphene nanoplatelets play the best stiffening effect in FDM printed parts when the deposited layers are aligned along the tensile load direction. It is worthwhile to note that the presence of graphene also causes a shift in loss modulus (E'') peak temperature by about two degrees (see Table 4) for all investigated samples. At the same time, a slight enlargement of width of loss modulus peak in graphene–ABS composite indicates the coexistence of differently constrained polymer chains, probably due to the restriction of chain motion of ABS matrix in the surrounding of graphene platelets.

Thermal strain of various specimens is compared in Fig. 7. As a common feature, an almost linear increase with temperature is observed up to about 100 °C, then in proximity of T_g a steep increment of thermal strain indicates a transition into the rubbery state with a higher mobility of polymer chains. Eventually, after a relative maximum at about 110–120 °C, an abrupt contraction suggests the tendency to recover a random coil conformation. The values of coefficient of linear thermal expansion (CLTE) of ABS and ABS-xGnP nanocomposites for different processing routes and along various 3D-printing orientations have been calculated from the thermal strain, and summarized in Table 5. Four temperature ranges have been selected in the glassy zone, i.e. at low temperature ($\Delta T_1 = -50/-20$ °C), at room temperature ($\Delta T_2 = 20/50$ °C) and at high temperature close T_g ($\Delta T_3 = 70/90$ °C and $\Delta T_4 = 108°/113$ °C), respectively. CLTE values of neat ABS up to 50 °C are in the range 60–75 $\times 10^{-6}$/K, which are slightly lower than 90 $\times 10^{-6}$/K, the literature value of general purpose ABS [46]. After addition of xGnP nanoplatelets, CLTE is remarkably reduced with values in the range 44–66 $\times 10^{-6}$/K, which means a better thermal stability in all the temperature intervals. In particular, xGnP causes a reduction of CLTE of about 15% for CM specimen and about 42% for extruded specimen.

FDM specimens (H, V and P) printed with neat ABS, present room temperature CLTE values of 66–74 $\times 10^{-6}$/K (Table 5), comparable to the values of 78–87 $\times 10^{-6}$/K previously reported for FDM printed ABS [11,30]. After the dispersion of xGnP nanoplatelets CLTE at room temperature reduces by 26% and 27% for H and V specimens, whereas only 1% for P specimen, respectively. The

Table 4
Dynamic mechanical properties of neat ABS and its nanocomposites as measured on compression moulded (CM), extruded (E) and 3D-printed specimens with different orientations (H, V, P).

Sample	Storage modulus			Damping peaks		Loss modulus of SAN peak		
	−50 °C (MPa)	30 °C (MPa)	125 °C (MPa)	B-phase T_{g1} (°C)	SAN-phase T_{g2} (°C)	E''_{peak} (MPa)	T_{peak} (°C)	w_{peak}[a] (°C)
CM	2009	1769	6.1	−77.6	120.7	333	112.2	10.1
4-CM	2271	1995	12.3	−76.7	122.7	402	113.4	11.4
E	2191	1889	6.0	−80.1	120.2	316	110.5	12.5
4-E	2661	2337	14.0	−79.6	122.4	413	112.6	13.1
H	1871	1598	9.9	−76.9	123.3	286	113.5	12.6
4-H	2248	1975	27.3	−77.4	125.7	372	116.2	12.9
V	1611	1399	6.1	−76.6	120.7	275	112.4	11.2
4-V	2159	1883	15.3	−76.0	123.5	364	114.6	11.9
P	1517	1306	5.8	−76.8	121.7	235	112.8	11.2
4-P	1580	1371	11.4	−75.8	123.9	257	115.3	11.3

[a] Width at half peak.

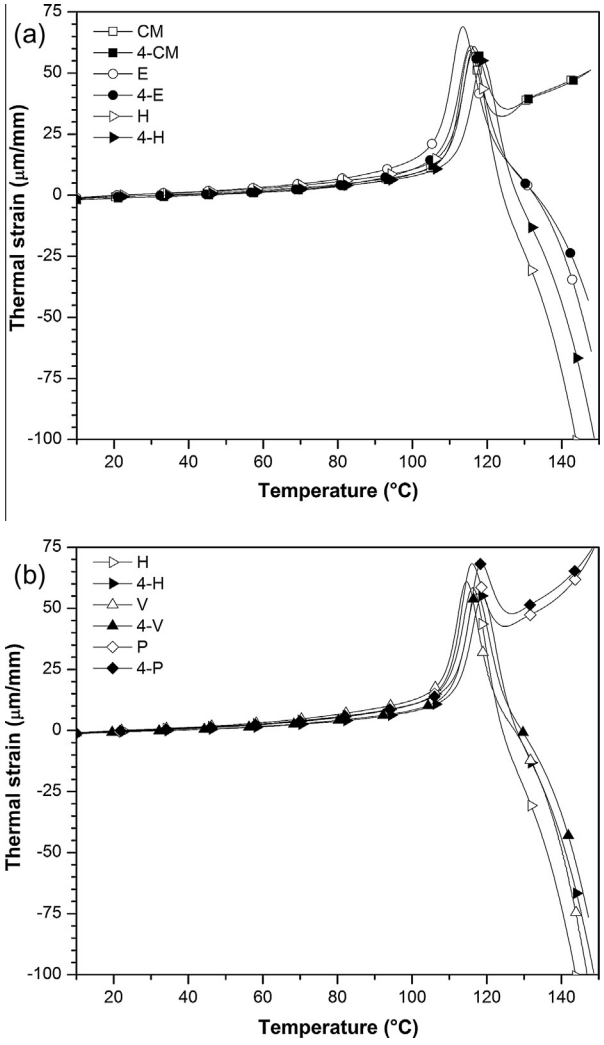

Fig. 7. Thermal strain of neat ABS and nanocomposite samples as measured on (a) compression moulded (CM), extruded (E) and 3D-printed specimens along horizontal orientation (H) and (b) along different orientations (H, V, P).

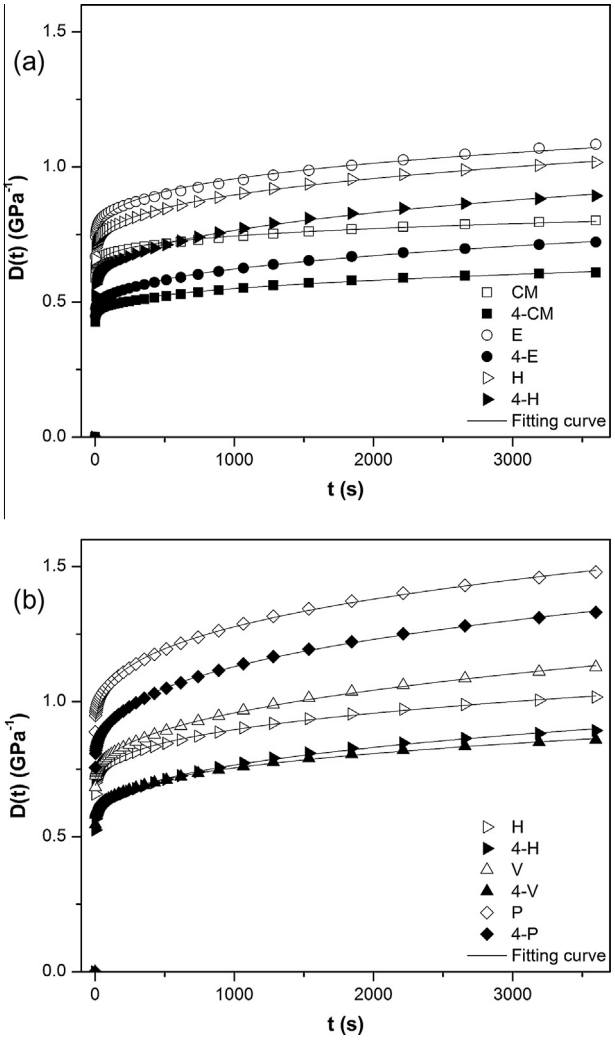

Fig. 8. Creep compliance, D(t) at 30 °C and 3.9 MPa, of neat ABS and nanocomposites as measured on a) compression moulded (CM), extruded (E) and 3D-printed specimens along horizontal orientation (H) and (b) along different orientations (H, V, P).

behaviour of P specimen indicates that the graphene nanoplatelets have an almost negligible effect on CLTE of ABS matrix, because in this case the main role is determined by the adhesion layer (see Fig. 3c). In the proximity of T_g (ΔT_4 = 108/113 °C) the effect of graphene on ABS matrix indicated a certain reduction of CLTE of CM and E specimens (about 25–30%), and a stronger variation for all FDM printed specimens (about 55% of CLTE reduction).

The thermal dilation behaviour above the glass transition temperature of SAN phase (range (ΔT_5 = 125 °C/150 °C) is described by the CLTD coefficients reported in the last column of Table 5. Poorly oriented samples, such as CM and P, show a positive thermal strain, corresponding to CLTD values of about 750 and 1250 $\times$ 10^{-6}/K for ABS, respectively, that slightly decrease (−7/12%) after graphene addition. On the other hand, negative CLTD values can be found

Table 5
Coefficients of linear thermal expansion (CLTE) and linear thermal deformation (CLTD) of ABS and its nanocomposites as measured on compression moulded (CM), extruded (E) and 3D-printed specimens with different orientations (H, V, P).

Sample	CLTE ($\times 10^{-6}$/K)				CLTD ($\times 10^{-6}$/K)
	ΔT_1 = −50/−20 °C	ΔT_2 = 20/50 °C	ΔT_3 = 70/90 °C	ΔT_4 = 108/113 °C	ΔT_5 = 120/150 °C
CM	62.0 ± 0.2	64.7 ± 0.2	159.7 ± 0.9	5784 ± 281	773 ± 8
4-CM	54.2 ± 0.1	54.9 ± 0.2	169.0 ± 1.2	4389 ± 180	678 ± 4
E	60.0 ± 0.2	74.7 ± 0.3	232.2 ± 2.1	8266 ± 111	−3292 ± 57
4-E	43.8 ± 0.1	43.3 ± 0.2	193.0 ± 1.9	5692 ± 179	−2475 ± 33
H	64.9 ± 0.1	65.5 ± 0.3	174.2 ± 0.9	4081 ± 144	−5722 ± 78
4-H	48.9 ± 0.1	48.3 ± 0.2	141.7 ± 0.9	1907 ± 62	−4466 ± 52
V	65.9 ± 0.1	73.5 ± 0.3	212.6 ± 0.9	6601 ± 209	−4854 ± 83
4-V	49.3 ± 0.1	53.7 ± 0.3	151.0 ± 0.7	2933 ± 112	−3768 ± 55
P	65.6 ± 0.1	66.3 ± 0.3	183.3 ± 1.2	5660 ± 217	1257 ± 24
4-P	60.4 ± 0.1	65.6 ± 0.3	187.4 ± 1.3	2476 ± 90	1169 ± 18

Table 6
Elastic (D_{el}), viscoelastic $D_{ve}(t = 3600\ s)$ and total $D(t = 3600\ s)$ creep compliance at 3600 s, and fitting parameters (Eq. (6)) of ABS and its nanocomposites as measured on compression moulded (CM), extruded (E) and 3D-printed specimens with different orientations (H, V, P).

Sample	D_{el} (GPa^{-1})	$D_{ve}(t = 3600s)$ (GPa^{-1})	$D(t = 3600s)$ (GPa^{-1})	D_e (GPa^{-1})	k ($GPa^{-1}\ s^{-n}$)	n	R^2
CM	0.59	0.21	0.80	0.576	0.037	0.219	0.9853
4-CM	0.43	0.18	0.61	0.437	0.010	0.345	0.9877
E	0.67	0.42	1.08	0.688	0.039	0.280	0.9786
4-E	0.45	0.27	0.72	0.454	0.013	0.371	0.9959
H	0.66	0.36	1.02	0.660	0.024	0.331	0.9950
4-H	0.53	0.37	0.89	0.532	0.020	0.356	0.9947
V	0.68	0.45	1.13	0.696	0.017	0.399	0.9961
4-V	0.55	0.31	0.86	0.543	0.023	0.323	0.9953
P	0.89	0.59	1.48	0.879	0.041	0.329	0.9968
4-P	0.76	0.57	1.33	0.742	0.039	0.333	0.9977

on extruded filaments and on FDM samples along H and V orientation. In this elevated temperature range, the reinforcing effect of graphene is markedly evident in the more oriented samples (E, H and V) with a shrinkage reduced by about 24% with respect of neat ABS. It is worthwhile to observe that nanofiller causes a reduction of both CLTE (below T_g) and CLTD (above T_g), suggesting an effective interaction between graphene and ABS both in the glassy and in the rubbery state.

3.6. Creep stability

Fig. 8a and b shows the isothermal creep compliance of neat ABS and relative nanocomposite. If no plastic deformation is produced in the course of creeping, the total creep compliance in isothermal tensile creep in the linear viscoelastic region, $D(t)$, is generally viewed as consisting of two components, (i) elastic (instantaneous, reversible), D_{el}, and (ii) viscoelastic (time-dependent, reversible) $D_{ve}(t)$ [47,48]:

$$D(t) = D_{el} + D_{ve}(t) \quad (5)$$

Elastic (D_{el}), viscoelastic $D_{ve}(t = 3600\ s)$ and total $D(t = 3600\ s)$ creep compliance at 3600 s have been estimated on creep curves and summarized in Table 6. It is evident that the addition of graphene nanoplatelets can promote the reduction of creep compliance for each investigated process and build orientation. The role of nanofiller is to restrict the polymeric chain mobility, thus promoting a better creep stability. According to the results, extrudate sample exhibits the highest reduction of creep compliance compared to compression moulded and printed specimens. For FDM printed specimens at various orientation, vertically built specimens show the highest reduction of creep compliance by about 24% owing to addition of xGnP.

To model the viscoelastic creep response Findley's model (power law) is commonly adopted to fit the experimental data [49]. This model can be obtained by expanding the Kohlrausch–Williams–Watts (KWW) model [50], generally described by a Weibull-like function as a series and ignoring all but the first term [51]:

$$D(t) = D_e + k\,t^n \quad (6)$$

where D_e is the elastic instantaneous creep compliance, k is a coefficient related to the magnitude of the underlying retardation process and n is an exponent tuning the time dependency of the creep process. The parameters resulting from best fitting of experimental creep data are summarized in Table 6. The elevated R^2 values indicate that the Findley equation can satisfactory represent the experimental data. The reduction of the creep compliance due to the addition of xGnP seems to be mostly associated to a reduction of the values of parameters D_e, which is comparable to D_{el} and k. In fact, the coefficient n, which represents the kinetics of the flow process of macromolecules during creep time, is only marginally affected by the presence of xGnP.

4. Conclusions

Graphene nanoplatelets were successfully melt compounded in an ABS matrix by using a completely solvent-free process, and then extruded in filaments suitable for fused deposition modelling. Due to the processing constraints, the filler content was optimized at 4 wt%. The thermo-mechanical properties of neat ABS and its nanocomposites have been compared on samples obtained through various processing routes such as compression moulding, extrusion and fused-deposition modelling. In all cases, the presence of graphene nanoplatelets improved the tensile modulus of ABS. This positive effect was also verified along several different orientations in FDM samples. Concurrently, the presence of xGnP causes a slight reduction of ultimate tensile stress and strain at break for horizontal and vertical 3D built specimens and a more severe effect along perpendicular direction. Moreover, xGnP was also proven to reduce the coefficient of thermal dilation of 3D printed parts and to improve their stability under long lasting loads. In fact, the creep compliance significantly reduced by addition of the nanofiller. For FDM-printed parts the graphene nanoplatelets resulted to play the best reinforcement effect for horizontal and vertical orientation and to be less effective for perpendicularly printed specimens.

Acknowledgments

S. Dul gratefully acknowledges the financial support by the Erasmus Mundus Action 2 Programme of the European Union, AREAS+ project.

References

[1] Wong KV, Hernandez A. A review of additive manufacturing. ISRN Mech Eng 2012;2012:1–10.
[2] Durgun I, Ertan R. Experimental investigation of FDM process for improvement of mechanical properties and production cost. Rapid Prototyp J 2014;20(3):228–35.
[3] Ivanova O, Williams C, Campbell T. Additive manufacturing (AM) and nanotechnology: promises and challenges. Rapid Prototyp J 2013;19(5):353–64.
[4] Dimitrov D, Schreve K, de Beer N. Advances in three dimensional printing – state of the art and future perspectives. Rapid Prototyp J 2006;12(3):136–47.
[5] Krawczak P. Additive manufacturing of plastic and polymer composite parts: promises and challenges of 3D-printing. Exp Pol Lett 2015;9(11):959.
[6] Hill N, Haghi M. Deposition direction-dependent failure criteria for fused deposition modeling polycarbonate. Rapid Prototyp J 2014;20(3):221–7.
[7] Hutmacher D, Schantz T, Zein I, Ng K, Teoh SH, Tan K. Mechanical properties and cell cultural response of polycaprolactone scaffolds designed and fabricated via fused deposition modeling. J Biomed Mater Res 2001;55(2):203–16.
[8] Ramanath HS, Chua CK, Leong KF, Shah KD. Melt flow behaviour of poly-epsilon-caprolactone in fused deposition modelling. J Mater Sci Mater Med 2008;19(7):2541–50.
[9] Shim J-H, Won J-Y, Sung S-J, Lim D-H, Yun W-S, Jeon Y-C, et al. Comparative efficacies of a 3D-printed PCL/PLGA/β-TCP membrane and a titanium membrane for guided bone regeneration in Beagle Dogs. Polymers 2015;7(10):2061–77.

[10] Leigh SJ, Bradley RJ, Purssell CP, Billson DR, Hutchins DA. A simple, low-cost conductive composite material for 3D printing of electronic sensors. PLoS One 2012;7(11):e49365.
[11] Love LJ, Kunc V, Rios O, Duty CE, Elliott AM, Post BK, et al. The importance of carbon fiber to polymer additive manufacturing. J Mater Res 2014;29 (17):1893–8.
[12] Tekinalp HL, Kunc V, Velez-Garcia GM, Duty CE, Love LJ, Naskar AK, et al. Highly oriented carbon fiber–polymer composites via additive manufacturing. Compos Sci Technol 2014;105:144–50.
[13] Torrado Perez AR, Roberson DA, Wicker RB. Fracture surface analysis of 3D-printed tensile specimens of novel ABS-based materials. J Fail Anal Prevent 2014;14(3):343–53.
[14] Campbell TA, Ivanova OS. 3D printing of multifunctional nanocomposites. Nano Today 2013;8(2):119–20.
[15] Postiglione G, Natale G, Griffini G, Levi M, Turri S. UV-assisted three-dimensional printing of polymer nanocomposites based on inorganic fillers. Polym Compos 2015.
[16] Zhong W, Li F, Zhang Z, Song L, Li Z. Short fiber reinforced composites for fused deposition modeling. Mater Sci Eng, A 2001;301(2):125–30.
[17] Shofner ML, Lozano K, Rodriguez-Macias FJ, Barrera EV. Nanofiber-reinforced polymers prepared by fused deposition modeling. J Appl Polym Sci 2003;89 (11):3081–90.
[18] Farahani RD, Dalir H, Le Borgne V, Gautier LA, El Khakani MA, Levesque M, et al. Direct-write fabrication of freestanding nanocomposite strain sensors. Nanotechnology 2012;23(8):085502.
[19] Farahani RD, Dalir H, Le Borgne V, Gautier LA, El Khakani MA, Lévesque M, et al. Reinforcing epoxy nanocomposites with functionalized carbon nanotubes via biotin–streptavidin interactions. Compos Sci Technol 2012;72(12):1387–95.
[20] Guo S-Z, Yang X, Heuzey M-C, Therriault D. 3D printing of a multifunctional nanocomposite helical liquid sensor. Nanoscale 2015;7(15):6451–6.
[21] Postiglione G, Natale G, Griffini G, Levi M, Turri S. Conductive 3D microstructures by direct 3D printing of polymer/carbon nanotube nanocomposites via liquid deposition modeling. Compos Part A Appl Sci Manuf 2015;76:110–4.
[22] Compton BG, Lewis JA. 3D-printing of lightweight cellular composites. Adv Mater 2014;26(34):5930–5.
[23] Duguay A, Nader J, Kiziltas A, Gardner D, Dagher H. Exfoliated graphite nanoplatelet-filled impact modified polypropylene nanocomposites: influence of particle diameter, filler loading, and coupling agent on the mechanical properties. Appl Nanosci 2014;4(3):279–91.
[24] Jiang X, Drzal LT. Multifunctional high density polyethylene nanocomposites produced by incorporation of exfoliated graphite nanoplatelets 1: morphology and mechanical properties. Polym Compos 2010;31(6):1091–8.
[25] Kalaitzidou K, Fukushima H, Drzal LT. Multifunctional polypropylene composites produced by incorporation of exfoliated graphite nanoplatelets. Carbon 2007;45(7):1446–52.
[26] Kim M, Hwang S-H, Kim B-J, Baek J-B, Shin HS, Park HW, et al. Modeling, processing, and characterization of exfoliated graphite nanoplatelet-nylon 6 composite fibers. Compos Part B Eng 2014;66:511–7.
[27] Li B, Zhong WH. Review on polymer/graphite nanoplatelet nanocomposites. J Mater Sci 2011;46(17):5595–614.
[28] Pedrazzoli D, Pegoretti A. Expanded graphite nanoplatelets as coupling agents in glass fiber reinforced polypropylene composites. Compos Part A Appl Sci Manuf 2014;66:25–34.
[29] Thanh TD, Kaprálková L, Hromádková J, Kelnar I. Effect of graphite nanoplatelets on the structure and properties of PA6-elastomer nanocomposites. Eur Polym J 2014;50:39–45.
[30] Wei X, Li D, Jiang W, Gu Z, Wang X, Zhang Z, et al. 3D printable graphene composite. Sci Rep 2015;5:11181.
[31] ASTM Standard D123 – 15b standard terminology relating to textiles.
[32] Mohamed OA, Masood SH, Bhowmik JL. Optimization of fused deposition modeling process parameters: a review of current research and future prospects. Adv Manuf 2015;3(1):42–53.
[33] Fambri L, Bragagna S, Migliaresi C. Biodegradable fibers of poly-L, DL-lactide 70/30 produced by melt spinning. Macromol Symposia 2006;234(1):20–5.
[34] Sun Q, Rizvi GM, Bellehumeur CT, Gu P. Effect of processing conditions on the bonding quality of FDM polymer filaments. Rapid Prototyp J 2008;14 (2):72–80.
[35] Blom H, Yeh R, Wojnarowski R, Ling M. Detection of degradation of ABS materials via DSC. Thermochim Acta 2006;442(1):64–6.
[36] Rytlewski P, Moraczewski K, Żenkiewicz M. Effects of coffee on the stability of accelerated aged poly(acrylonitryle–butadiene–styrene). J Appl Polym Sci 2014;131(4):n/a–a.
[37] Reed TF, Bair HE, Vadimsky RG. The causes of pitting and haze on molded ABS plastic surfaces. In: Sperling L, editor. Recent advances in polymer blends, grafts, and blocks. New York: Plenum Press; 1974. p. 359–73.
[38] Ahn S-H, Montero M, Odell D, Roundy S, Wright PK. Anisotropic material properties of fused deposition modeling ABS. Rapid Prototyp J 2002;8 (4):248–57.
[39] Valentan B, Pogacar D, Brajlih T, Hartner TZ, Pilipovic A, Drstvensek I. Development of a 3D printer for thermoplastic modelling. Mater Technol 2012;46(6):589–94.
[40] Jami H, Masood SH, Song WQ. Dynamic response of FDM made ABS parts in different part orientations. Adv Mater Res 2013;748:291–4.
[41] Riccò T, Pavan A, Danusso F. Dynamic transition of grafted polybutadiene in ABS resins. Polymer 1975;16:685–9.
[42] Mas J, Vidaurre A, Meseguer JM, Romero F, Pradas MM, Ribelles JLG, et al. Dynamic mechanical properties of polycarbonate and acrylonitrile–butadiene–styrene copolymer blends. J Appl Polym Sci 2002;83(7):1507–16.
[43] Sepe MP. Dynamic mechanical analysis for plastics engineering. Norwich, New York: Plastics Design Library; 1998.
[44] Tiganis BE, Burna LS, Davisa P, Hillb AJ. Thermal degradation of acrylonitrile–butadiene–styrene ABS) blends. Polym Degrad Stab 2002;76(3):425–43.
[45] Arivazhagan A, Masood SH. Dynamic mechanical properties of ABS material processed by fused deposition modelling. Int J Eng Res Appl 2012;2 (3):2009–14.
[46] Crawford R. Plastics engineering. 3rd ed. Oxford: Butterworth-Heinemann; 1998.
[47] Kolarik J, Pegoretti A. Proposal of the Boltzmann-like superposition principle for nonlinear tensile creep of thermoplastics. Polym Test 2008;27(5):596–606.
[48] Dorigato A, Pegoretti A, Kolarik J. Nonlinear tensile creep of linear low density polyethylene/fumed silica nanocomposites: time–strain superposition and creep prediction. Polym Compos 2010;31(11):1947–55.
[49] Pegoretti A. Creep and fatigue behaviour of polymer nanocomposites. In: Karger-Kocsis J, Fakirov S, editors. Nano- and micromechanics of polymer blends and composites. Munich (Germany): Carl Hanser Verlag GmbH & Co. KG; 2009. p. 301–39.
[50] Williams G, Watts D. Non-symmetrical dielectric relaxation behaviour arising from a simple empirical decay function. Trans Faraday Soc 1970;66:80–5.
[51] Findley W. 26-Year creep and recovery of poly(vinyl chloride) and polyethylene. Polym Eng Sci 1987;27(8):582–5.